U.S. Department of Transportation

Federal Railroad Administration

Track Profile Approximation Using Railcar Body Acceleration Data

Office of Research
and Development
Washington, DC 20590

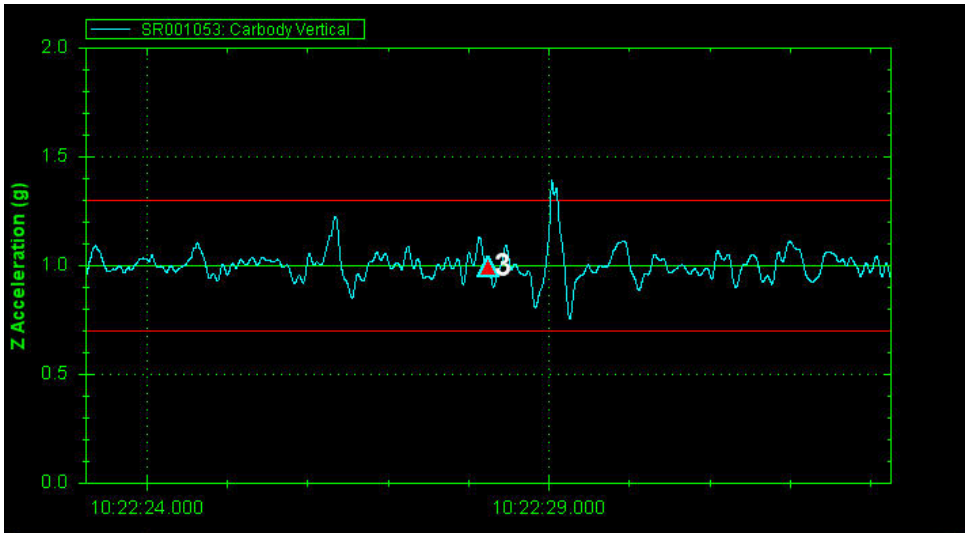

DOT/FRA/ORD-14/42

Final Report
December 2014

NOTICE

This document is disseminated under the sponsorship of the Department of Transportation in the interest of information exchange. The United States Government assumes no liability for its contents or use thereof. Any opinions, findings and conclusions, or recommendations expressed in this material do not necessarily reflect the views or policies of the United States Government, nor does mention of trade names, commercial products, or organizations imply endorsement by the United States Government. The United States Government assumes no liability for the content or use of the material contained in this document.

NOTICE

The United States Government does not endorse products or manufacturers. Trade or manufacturers' names appear herein solely because they are considered essential to the objective of this report.

REPORT DOCUMENTATION PAGE

Form Approved
OMB No. 0704-0188

1. AGENCY USE ONLY (Leave blank)	2. REPORT DATE	3. REPORT TYPE AND DATES COVERED
	December 2014	Technical Report

4. TITLE AND SUBTITLE
Track Profile Approximation Using Railcar Body Acceleration Data

5. FUNDING NUMBERS

6. AUTHOR(S)
Leith Al-Nazer

7. PERFORMING ORGANIZATION NAME(S) AND ADDRESS(ES)
U.S. Department of Transportation
Federal Railroad Administration
Office of Railroad Policy and Development
Office of Research and Development
Washington, DC 20590

8. PERFORMING ORGANIZATION REPORT NUMBER

9. SPONSORING/MONITORING AGENCY NAME(S) AND ADDRESS(ES)
U.S. Department of Transportation
Federal Railroad Administration
Office of Railroad Policy and Development
Office of Research and Development
Washington, DC 20590

10. SPONSORING/MONITORING AGENCY REPORT NUMBER
DOT/FRA/ORD-14/42

11. SUPPLEMENTARY NOTES

12a. DISTRIBUTION/AVAILABILITY STATEMENT
This document is available to the public through the FRA Web site at http://www.fra.dot.gov.

12b. DISTRIBUTION CODE

13. ABSTRACT (Maximum 200 words)
Accelerations are frequently measured from the car body of a rail vehicle, which is mounted above one or more suspension systems. Measuring accelerations in the car body is largely done for convenience, as mounting an accelerometer to a truck or axle of a railcar is more cumbersome than simply placing an accelerometer inside the railcar body. For those involved with track research, maintenance, and safety, there is a desire to correlate these car body accelerations with track conditions. However, a railcar suspension system acts as a filter that can interfere with taking precise acceleration measurements. To complicate matters further, the railcar body, in combination with the suspension system, has several natural modes of vibrations. As a result, some accelerations that exceed a predefined threshold measured from the railcar body do not correlate with track conditions. Thus, the use of acceleration data in this manner to accurately and reliably identify track defects or exceptions may be hampered--potentially triggering further inspection by railroad personnel when unnecessary--or masking such indicators. This report puts forth a simplified model of a railcar and a corresponding deconvolution filter (also known as an inverse filter) which theoretically eliminates the amplification and attenuation effects of the railcar suspension system.

14. SUBJECT TERMS
Track geometry, vehicle-track interaction, ride quality

15. NUMBER OF PAGES
43

16. PRICE CODE

17. SECURITY CLASSIFICATION OF REPORT	18. SECURITY CLASSIFICATION OF THIS PAGE	19. SECURITY CLASSIFICATION OF ABSTRACT	20. LIMITATION OF ABSTRACT
Unclassified	Unclassified	Unclassified	

METRIC/ENGLISH CONVERSION FACTORS

ENGLISH TO METRIC	METRIC TO ENGLISH
LENGTH (APPROXIMATE)	**LENGTH (APPROXIMATE)**
1 inch (in) = 2.5 centimeters (cm)	1 millimeter (mm) = 0.04 inch (in)
1 foot (ft) = 30 centimeters (cm)	1 centimeter (cm) = 0.4 inch (in)
1 yard (yd) = 0.9 meter (m)	1 meter (m) = 3.3 feet (ft)
1 mile (mi) = 1.6 kilometers (km)	1 meter (m) = 1.1 yards (yd)
	1 kilometer (km) = 0.6 mile (mi)
AREA (APPROXIMATE)	**AREA (APPROXIMATE)**
1 square inch (sq in, in^2) = 6.5 square centimeters (cm^2)	1 square centimeter (cm^2) = 0.16 square inch (sq in, in^2)
1 square foot (sq ft, ft^2) = 0.09 square meter (m^2)	1 square meter (m^2) = 1.2 square yards (sq yd, yd^2)
1 square yard (sq yd, yd^2) = 0.8 square meter (m^2)	1 square kilometer (km^2) = 0.4 square mile (sq mi, mi^2)
1 square mile (sq mi, mi^2) = 2.6 square kilometers (km^2)	10,000 square meters (m^2) = 1 hectare (ha) = 2.5 acres
1 acre = 0.4 hectare (he) = 4,000 square meters (m^2)	
MASS - WEIGHT (APPROXIMATE)	**MASS - WEIGHT (APPROXIMATE)**
1 ounce (oz) = 28 grams (gm)	1 gram (gm) = 0.036 ounce (oz)
1 pound (lb) = 0.45 kilogram (kg)	1 kilogram (kg) = 2.2 pounds (lb)
1 short ton = 2,000 pounds (lb) = 0.9 tonne (t)	1 tonne (t) = 1,000 kilograms (kg)
	= 1.1 short tons
VOLUME (APPROXIMATE)	**VOLUME (APPROXIMATE)**
1 teaspoon (tsp) = 5 milliliters (ml)	1 milliliter (ml) = 0.03 fluid ounce (fl oz)
1 tablespoon (tbsp) = 15 milliliters (ml)	1 liter (l) = 2.1 pints (pt)
1 fluid ounce (fl oz) = 30 milliliters (ml)	1 liter (l) = 1.06 quarts (qt)
1 cup (c) = 0.24 liter (l)	1 liter (l) = 0.26 gallon (gal)
1 pint (pt) = 0.47 liter (l)	
1 quart (qt) = 0.96 liter (l)	
1 gallon (gal) = 3.8 liters (l)	
1 cubic foot (cu ft, ft^3) = 0.03 cubic meter (m^3)	1 cubic meter (m^3) = 36 cubic feet (cu ft, ft^3)
1 cubic yard (cu yd, yd^3) = 0.76 cubic meter (m^3)	1 cubic meter (m^3) = 1.3 cubic yards (cu yd, yd^3)
TEMPERATURE (EXACT)	**TEMPERATURE (EXACT)**
[(x-32)(5/9)] °F = y °C	[(9/5) y + 32] °C = x °F

QUICK INCH - CENTIMETER LENGTH CONVERSION

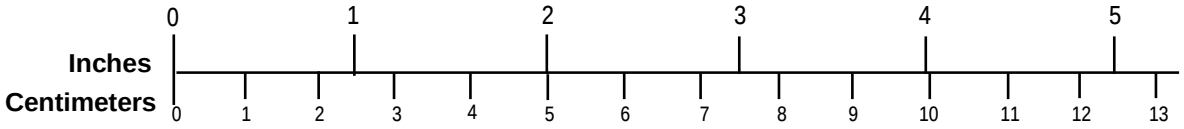

QUICK FAHRENHEIT - CELSIUS TEMPERATURE CONVERSIO

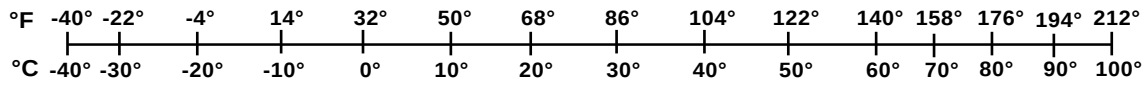

For more exact and or other conversion factors, see NIST Miscellaneous Publication 286, Units of Weights and Measures. Price $2.50 SD Catalog No. C13 10286

Updated 6/17/98

Acknowledgements

The author would like to acknowledge the support of Michael Trosino of Amtrak's engineering department for providing access to Amtrak's geometry car for data collection purposes.

In addition, the author would like to thank Dr. Thomas Raslear (Chief of FRA's Human Factors Research Division) for his edits to the sections of the report that deal with signal detection theory and statistics concepts.

Contents

Illustrations

Tables

Executive Summary

Measuring accelerations on railcars is an increasingly common practice among those involved with track research, maintenance, and safety because these acceleration measurements provide means for finding anomalous track conditions. Accelerations are oftentimes measured from the car body of a rail vehicle, which is mounted above one or more suspension systems. Measuring accelerations in the car body is largely done for convenience, as mounting an accelerometer to a truck or axle of a railcar is more cumbersome than simply placing an accelerometer inside the railcar body. However, a railcar suspension system acts as a filter which passes low frequencies and attenuates high frequencies. To complicate matters further, the railcar body, in combination with the suspension system, has several natural modes of vibrations. The mode of interest in this report is the vertical natural frequency, which is commonly known as the "bounce" mode of the vehicle.

As a result of this vertical natural frequency, some vertical accelerations measured from the railcar body that exceed a predefined threshold do not correlate with track conditions. Such events can be viewed as false alarms (or false positives) since an exception was measured on the car body but no significant defective track condition exists.[1] In addition, higher frequency accelerations due to high frequency impacts, for example, are attenuated by the suspension system, and accelerations exceeding the predefined threshold may not be recorded in the acceleration measurements taken on the car body. Such events can be classified as misses (or false negatives). For obvious reasons, track inspectors and maintenance personnel wish to minimize such spurious or erroneous readings. This report puts forth a simplified model of a railcar and a corresponding filter, known as a deconvolution filter, which theoretically eliminates, or at least reduces, the amplification and attenuation effects of the railcar suspension system. This modification allows the system to obtain an approximation of the unsprung mass accelerations and displacements, which are those experienced below the suspension system by an unsprung mass, such as the truck or axle of a railcar.

The effectiveness of the deconvolution filter at finding vertical track deviations (known as track profile deviations or track surface deviations) was determined by collecting vertical railcar body acceleration data on one of Amtrak's geometry cars. The exception locations output by the deconvolution filter were compared with the profile exceptions output by Amtrak's geometry car, and signal detection theory was used to quantify the effectiveness of the deconvolution filter at detecting track profile exception locations output by the geometry car. The results are promising and represent a substantial improvement over the traditional method of simply using peak-to-peak thresholds of low-pass filtered railcar body accelerations to detect defective track profile conditions.

Future efforts will be directed at further demonstrating the potential advantages and benefits of the deconvolution filter. For example, repeatability of the filter's function on two different railcars in the same consist may be investigated. In addition, researchers may evaluate the performance of the deconvolution filter on vertical acceleration data collected on other types of railcars besides passenger railcars.

[1] An "exception" refers to an event in which a predefined threshold is exceeded.

1. Introduction

1.1 Background and Objectives

Measuring accelerations on railcars is an increasingly common practice among those involved with track research, maintenance, and safety because these acceleration measurements provide means for finding anomalous track conditions. Accelerations are oftentimes measured from the car body of a rail vehicle, which is mounted above one or more suspension systems. Measuring accelerations on the body of a railcar is largely done for convenience, as mounting an accelerometer to a truck or axle of a railcar is more cumbersome than simply placing an accelerometer inside the railcar body. However, a railcar suspension system acts as a filter which passes low frequencies and attenuates high frequencies. To complicate matters further, the railcar body, in combination with the suspension system, has several natural modes of vibrations. The mode of interest in this report is the vertical natural frequency, which is commonly known as the "bounce" mode of the vehicle.

Because of this vertical natural frequency, some vertical accelerations measured from the railcar body which exceed a predefined threshold do not correlate with track conditions. Such events can be viewed as false alarms (or false positives) since an exception was measured on the car body but no significant defective track condition exists.[2] In addition, higher frequency accelerations due to high frequency impacts, for example, are attenuated by the suspension system, and accelerations exceeding the predefined threshold may not be reflected in acceleration measurements taken on the car body. Such events can be classified as misses (or false negatives). An approach to minimize such misses and false alarms is desired. This report puts forth a simplified model of a railcar and a corresponding filter, known as a deconvolution filter, which theoretically eliminates, or at least reduces, the amplification and attenuation effects of the railcar suspension system. This new model therefore allows researchers to obtain an approximation of the unsprung mass accelerations and displacements, which are the accelerations and displacements experienced below the suspension system by an unsprung mass such as the truck or axle of a railcar.

GPS systems are currently very common and affordable and are relevant to the application of a deconvolution filter because they can provide approximate speed of the vehicle on which railcar body accelerations are being measured. Knowing the speed of the vehicle allows for the conversion from time as the independent variable to distance as the independent variable. In addition to unsprung mass accelerations, the deconvolution filter also outputs unsprung mass vertical velocity and unsprung mass vertical displacement. Presenting the unsprung mass displacement as a function of distance, rather than time, allows for approximation of the vertical track geometry[3] of the overall track. Obtaining vertical track geometry as an output is important because Federal regulations put forth in 49 CFR 213 (otherwise known as the "Track Safety Standards") lay out specific standards and thresholds for track geometry.

---

[2] An "exception" refers to an event in which a predefined threshold is exceeded.

[3] "Track geometry" is a railroad term that refers to the vertical and lateral displacement of each of the rails with respect to distance. In other words, the term refers to the vertical and lateral deviations of the left rail and the right rail in space.

In summary, application of the deconvolution filter to measured railcar body vertical accelerations, coupled with speed information obtained with a GPS sensor, allows for the construction of an approximate vertical track geometry signal, which is important for the maintenance and safety of railroad operations. Furthermore, the deconvolution filter provides a method to obtain this acceleration information using a single-axis accelerometer, a GPS positioning sensor, and easily portable hardware.

1.2 Organization of the Report

Section 2 of the report identifies the assumptions regarding the physical characteristics of the railcar. Section 3 uses the assumptions put forth in Section 2 to design a deconvolution filter. Section 4 shows some preliminary results of applying the deconvolution filter to measured railcar body accelerations. Section 5 documents a data collection effort that took place on Amtrak's geometry car as well as the results of the data analysis effort that followed. Section 6 provides some concluding remarks.

2. Simplified Railcar Model

For the purposes of this analysis, the railcar will be modeled simply as a linear, damped, harmonic oscillator. This is a single degree of freedom model which only takes into consideration rigid body vertical displacements. The model consists of a mass, a linear spring, and a linear viscous damper (Figure 1).

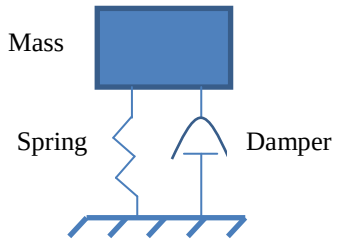

Figure 1. Mass-spring-damper system

Despite its simplicity, the model might suffice for the purposes of more accurately correlating vertical track geometry deviations (also known as "track surface" or "track profile" deviations) with measured vertical railcar body accelerations, as will become more evident in the discussion of the deconvolution filter in the following sections. However, due to the linearity assumption, the model being used more accurately applies to a well-performing suspension system, such as the suspension system of a passenger railcar; the suspension system of freight cars are oftentimes highly non-linear. A more complex model that takes into account multiple modes of vibration (bounce and pitch, for example) may be used, and the overall methodology of the analysis presented in this paper could still be applied as long as the model being used is linear. A model with multiple modes of vibration will most likely require accelerometers to be used at multiple locations on the car. Using the simplified single mode vibration model requires using only a single accelerometer.

Ideally, the accelerometer would be placed in the car body directly above one of the trucks. This placement would allow the accelerometer to receive as much of the input signal from the track as possible. If the accelerometer were placed a significant distance from either truck, it is likely that the input signal from the track would be significantly attenuated because of damping from non-rigid deformation modes of the railcar body. Since the current approach only considers vertical accelerations, any reference to "accelerations" or "displacements" in the rest of this paper refers to vertical accelerations and vertical displacements, unless otherwise stated.

The linear harmonic oscillator model used in this analysis is represented mathematically as a linear, second-order ordinary differential equation:[4]

[4] Further explanation of this equation can be found in textbooks, such as the introductory textbook by Rao (1986), on mechanical vibrations.

$$m\frac{d^2y}{dt^2}+c\frac{dy}{dt}+ky(t)=kf_{IN}(t)+c\frac{df_{IN}}{dt}$$

Equation 1

m is the mass of the body, *c* is the damping coefficient, and *k* is the spring stiffness. *y(t)* is the displacement of the harmonic oscillator sprung mass. $f_{IN}(t)$ represents the vertical displacement of the track with respect to time and may be thought of as the average vertical displacement of the left and right rails.

The characteristics of the harmonic oscillator, including transient response and steady state response, are determined primarily by the natural frequency, as well as the damping ratio.[5] The natural frequency of the railcar can be estimated using a Fast Fourier Transform (FFT) algorithm. The mass of a railcar vehicle is typically known (or can be estimated) and then the spring constant can be calculated using Equation 2.

$$\omega_n=\sqrt{\frac{k}{m}}$$

Equation 2

ω_n is the natural frequency in radians per second. Freight railcars and locomotives typically have a natural frequency of about 2 Hz (12.6 radians per second) in the rigid body vertical displacement mode, and passenger railcars typically have a natural frequency around 1.5 Hz (9.4 radians per second). The data analysis portion of this report will deal with data collected on a passenger railcar. Figure 2 shows an example FFT of the data that was collected on this passenger railcar. As shown, the natural frequency appears to be approximately 1.4 Hz. Therefore, for the purposes of this analysis, a natural frequency of 1.4 Hz (8.8 radians per second) will be assumed.

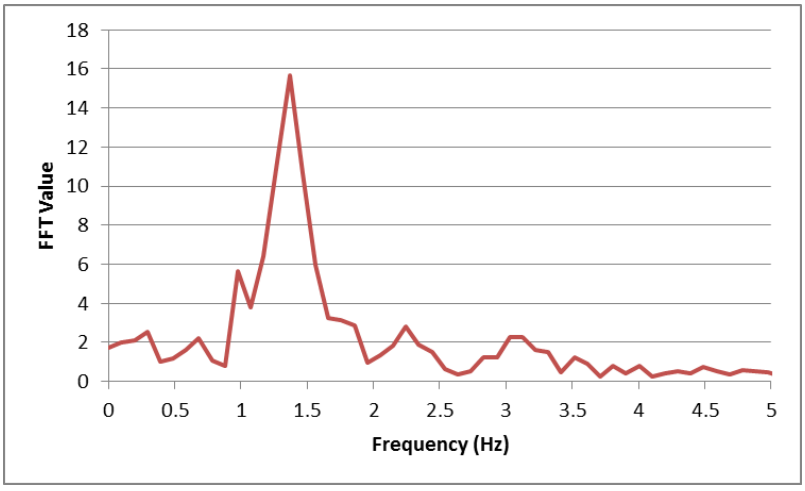

Figure 2. Results of performing FFT on measured acceleration data

[5] Further explanation of these terms can be found in introductory textbooks on mechanical vibrations, such as Rao (1986) or Hartog (1985).

The weights of railcars vary greatly. Typically, however, accelerations are measured from a locomotive or passenger railcar. A typical locomotive or loaded freight railcar weighs between 300,000 and 400,000 lb, and a typical passenger railcar weighs between 100,000 and 200,000 lb. As stated previously, the data analysis portion of this report deals with data collected on a passenger railcar, so a numerical value of 130,000 lb (~59,000 kg) will be assumed in this analysis.

The spring coefficient *k* can be determined by using Equation 2 and solving for *k*. Plugging in the appropriate numerical values results in a value of approximately 4,569,000 kg/s^2 for *k*. The critical damping value can be calculated using Equation 3.

$$c_{critical} = 2m\sqrt{\frac{k}{m}}$$

Equation 3

Plugging in the appropriate values for *k* and *m* results in a value of 1,038,400 kg/s for $c_{critical}$.

The damping ratio can be estimated by examining the vertical transient response of the railcar on which data is being collected. Figure 3, Figure 4, and Figure 5 show plots of measured and modeled transient response. The measured transient response (red plot) is the same in each of the three figures. This data was collected on the passenger railcar used for data collection purposes (see Section 5). However, the modeled transient response (purple plot) varies between each of the three figures. Figure 3 shows the modeled transient response of a harmonic oscillator assuming a damping ratio of 5 percent. Figure 4 and Figure 5 show the same plots for damping ratios of 15 percent and 25 percent, respectively.

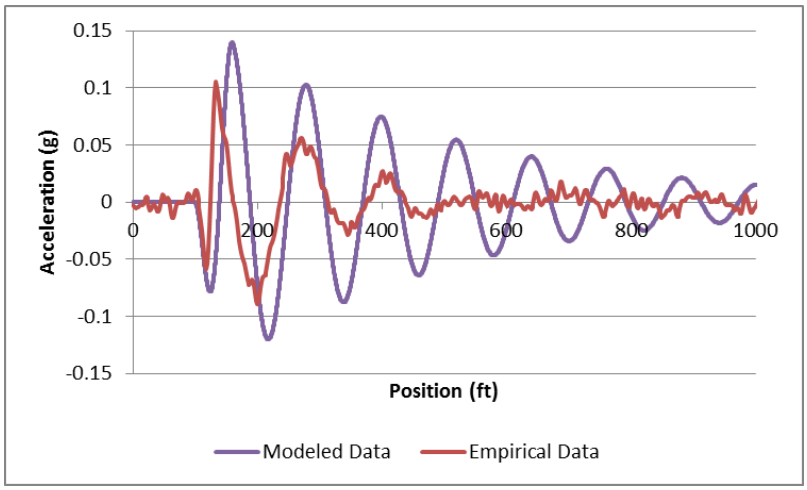

Figure 3. Modeled transient response with 5 percent damping ratio

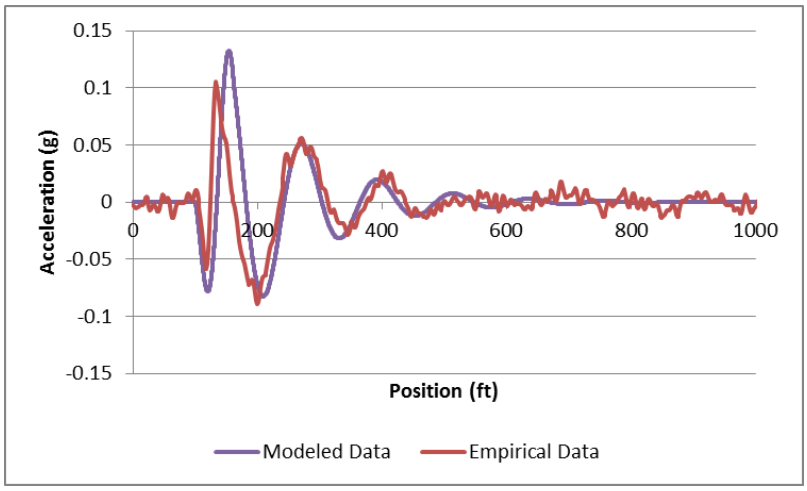

Figure 4. Modeled transient response with 15 percent damping ratio

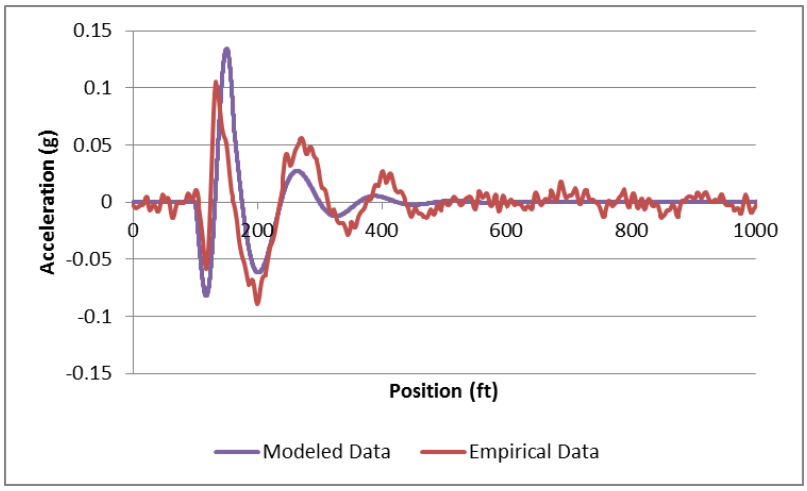

Figure 5. Modeled transient response with 25 percent damping ratio

As the results show, the best visual match appears to be with the 15 percent damping ratio (Figure 4). Therefore, a damping ratio of 0.15 will be assumed, and a damping value of 155,760 kg/s, which is 15 percent of the critical damping value, will be used for *c*. Table 1 summarizes the numerical values assigned to the various physical constants.

Table 1. Numerical values of physical constants

Physical Constant	Numerical Value
Mass m (kg)	59,000[6]
Stiffness k (kg/s^2)	4,569,000
Critical damping $c_{critical}$ (kg/s)	1,038,400
Damping Ratio	0.15
Damping c (kg/s)	155,760

The plot in Figure 6 represents the frequency response of the linear harmonic oscillator with the prescribed values for m, c, and k in Table 1. The frequency response plot clearly shows that there is a predominant natural frequency, and frequencies above the natural frequency are attenuated. These characteristics are typical of damped, linear harmonic oscillators. Figure 7 shows the same plot in log-log coordinates.

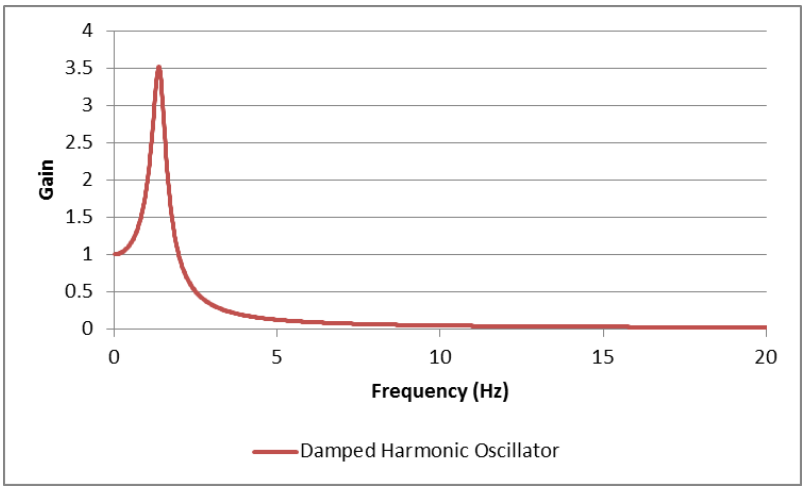

Figure 6. Frequency response of damped harmonic oscillator

[6] It is interesting to note that the mass of the railcar does not have to be estimated. In other words, any number could be used for the mass m. Once the natural frequency ω_n is specified and a mass m is assumed, then the spring stiffness k can be calculated using Equation 2, and the critical damping value $c_{critical}$ can be calculated using Equation 3. For example, setting ω_n to 8.8 radians per and the damping ratio to 0.15, then assuming a mass m, and finally calculating the corresponding values for spring stiffness k and critical damping value $c_{critical}$, a harmonic oscillator with the frequency response shown in Figure 6 and Figure 7 will result.

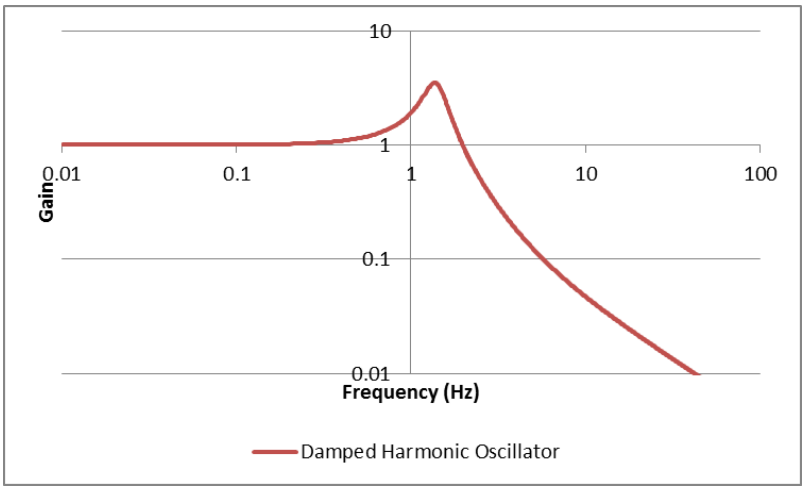

Figure 7. Frequency response of damped harmonic oscillator in log-log coordinates

3. Deconvolution Filter Design

In order to remove the effects of the railcar's suspension system, a filter must be designed with a gain which, when multiplied by the gain of the damped harmonic oscillator (Figure 7), will produce a resultant gain of unity for all the frequencies of interest. Such a filter is called a deconvolution filter[7] (also referred to as an inverse filter), and it can be achieved using Laplace transform theory and pole-zero plots.

Figure 8 shows a simple block diagram approach to the overall setup of the problem. Signal A represents the input to the harmonic oscillator. Signal B represents the output of the harmonic oscillator and the input to the deconvolution filter. Signal C represents the output of the deconvolution filter. Signal C is an approximate reconstruction of Signal A. In other words, the deconvolution filter is designed to transform Signal B back into Signal A. In real-world implementation, due to model inaccuracies, the inevitable presence of noise, and the effects of discrete-time sampling, the output of the deconvolution filter (Signal C) is not an exact replication of the original Signal A, but rather an approximation of the original Signal A input into the harmonic oscillator.

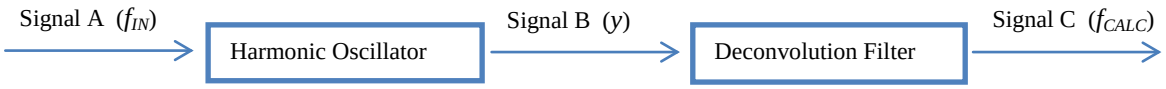

Figure 8. Block diagram of problem setup

Equation 4 represents the Laplace transform of the linear harmonic oscillator differential equation (Equation 1).

$$\left(ms^2 + cs + k\right)Y(s) = \left(cs + k\right)F_{IN}(s)$$

Equation 4

F_{IN} is the input to the harmonic oscillator (Signal A in Figure 8), and Y is the harmonic oscillator output (Signal B in Figure 8). The resulting transfer function is:

$$H_{HarmOsc}(s) = \frac{Y(s)}{F_{IN}(s)} = \frac{cs + k}{ms^2 + cs + k}$$

Equation 5

The zeros of the denominator are known as "poles," and the zeros of the numerator are known simply as "zeros." It is easy to visualize the poles and zeros by plotting them on an x-y plot where the x axis represents the real component of the poles and zeros, and the y axis represents the imaginary component of the poles and zeros. The numerical values of the poles and zeros used in this analysis are shown in Table 2 and are plotted in Figure 9. The real and imaginary

[7] More information on the mathematical theory of deconvolution and its applications can be found in technical textbooks, such as Lathi (2004), that cover the convolution integral and transform theory.

values for the poles and zeros put forth in Table 2 are based on the mass, damping, and stiffness values in Table 1.

Table 2. Real and imaginary components of damped harmonic oscillator poles and zeros

	Real Component	Imaginary Component
Pole #1	-1.3195	8.6969
Pole #2	-1.3195	8.6969
Zero #1	-29.3215	0.0000

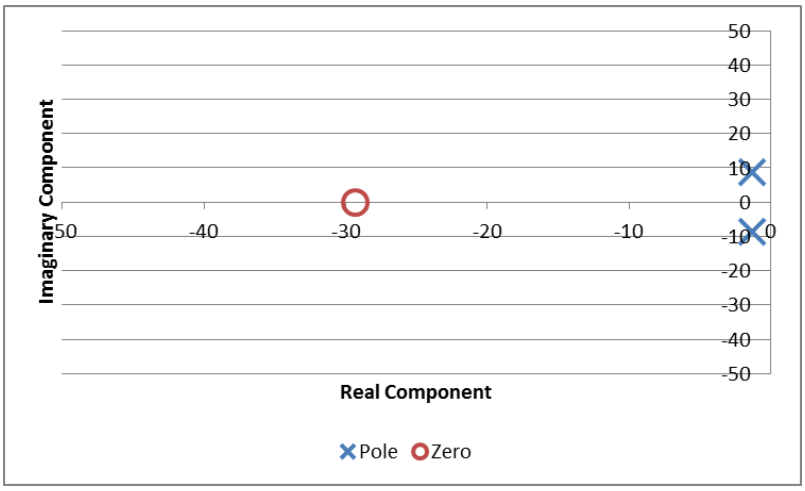

Figure 9. Pole-zero plot of damped harmonic oscillator

A deconvolution filter can be created by replacing all the poles with zeros and all the zeros with poles. However, this substitution results in more zeros than poles, and a stable filter requires more poles than zeros. Therefore, a plurality of poles should be added whose real components are equal to the desired high-frequency cutoff in radians per second. A numerical value of 6.5 Hz (or 34.5 radians per second) will be used as the cutoff frequency for this analysis. In order to achieve this cutoff frequency, six poles with a modulus[8] of 34.5 are placed in a Butterworth configuration (Pole #1 through Pole #6 in Table 3). The numerical values of all the deconvolution filter poles and zeros used in this analysis are shown in Table 3 and plotted in Figure 10.

[8] Most complete textbooks on complex variable theory provide an explanation of the term "modulus," as well as additional information on Laplace transform theory and filter design. A good textbook to consult is the complex variable textbook by LePage (1980).

Table 3. Real and imaginary components of deconvolution filter poles and zeros

	Real Component	Imaginary Component
Pole #1	-10.5704	39.4491
Pole #2	-10.5704	-39.4491
Pole #3	-28.8787	28.8787
Pole #4	-28.8787	-28.8787
Pole #5	-39.4491	10.5704
Pole #6	-39.4491	-10.5704
Pole #7	-29.3215	0.0000
Zero #1	-1.3195	8.6969
Zero #2	-1.3195	-8.6969

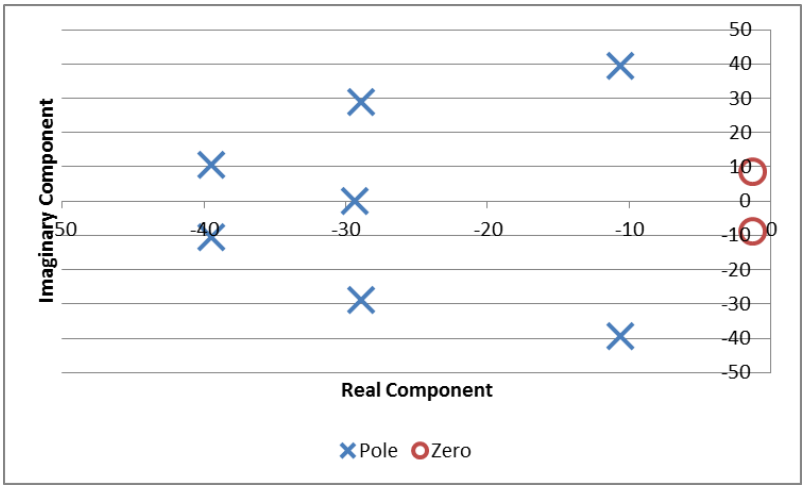

Figure 10. Pole-zero plot of deconvolution filter

Equation 6 represents the resulting transfer function of the deconvolution filter. Y is the input to the deconvolution filter (Signal B in Figure 8), and F_{CALC} is the output of the deconvolution filter (Signal C in Figure 8).

$$H_{DeconvFilter}(s) = G_{DeconvFilter}\frac{F_{CALC}(s)}{Y(s)}$$

$$= G_{DeconvFilter}\frac{(s+\beta_1)(s+\beta_2)}{(s+\alpha_1)(s+\alpha_2)(s+\alpha_3)(s+\alpha_4)(s+\alpha_5)(s+\alpha_6)\left(s+\frac{k}{c}\right)}$$

Equation 6

$G_{DeconvFilter}$ is the gain applied to the transfer function of the deconvolution filter in order to make the gain of the frequency response equal to 1 for frequencies approaching 0, as was the case for the frequency response of the harmonic oscillator (Figure 7). The numerical value for the gain of the deconvolution filter given the assumed physical constants (Table 1) and the 6.5 Hz frequency cutoff value is $1{,}758.451\times10^{6}$. α_1 through α_6 represent Pole #1 through Pole #6, respectively, in Table 3. $\frac{k}{c}$ represents Pole #7, and β_1 and β_2 represent Zero #1 and Zero #2, respectively (Table 3).

Multiplying through by the denominators results in:

$$\left((s+\alpha_1)(s+\alpha_2)(s+\alpha_3)(s+\alpha_4)(s+\alpha_5)(s+\alpha_6)\left(s+\frac{k}{c}\right)\right)F_{CALC}(s)=G_{DeconFilter}\left((s+\beta_1)(s+\beta_2)\right)Y(s)$$

Performing the necessary algebra and applying inverse Laplace transform techniques allows one to obtain the symbolic form of the governing differential equation of the deconvolution filter. Plugging in the numerical values in Table 1 and Table 3 results in the differential equation in Equation 7. The output *y(t)* from the harmonic oscillator (Equation 1) is the input to the deconvolution filter. The output of the deconvolution filter is labeled f_{CALC}.

$$\frac{d^7 f_{CALC}}{dt^7}+187.1\frac{d^6 f_{CALC}}{dt^6}+17076.7\frac{d^5 f_{CALC}}{dt^5}+987782.9\frac{d^4 f_{CALC}}{dt^4}+39025410.8\frac{d^3 f_{CALC}}{dt^3}+1047892980.3\frac{d^2 f_{CALC}}{dt^2}+$$
$$17512753599.3\frac{df_{CALC}}{dt}+136064866321.7\,f_{CALC}(t)=1758450677.0\frac{d^2 y}{dt^2}+4640442012.1\frac{dy}{dt}+136064866321.7\,y(t)$$

Equation 7

Figure 11 shows the frequency response plot of the damped harmonic oscillator and the deconvolution filter. Figure 12 also shows the frequency response but plotted in log-log coordinates. With these coordinates, it is easier to visualize the deconvolution filter as the "inverse" of the damped harmonic oscillator. The dotted purple line in Figure 11 and Figure 12 represents the product of the gain of the damped harmonic oscillator and the gain of the deconvolution filter. This value should be approximately unity across all the frequencies of interest, which for the purposes of this analysis are frequencies lower than 6.5 Hz. Assuming a damping ratio of 0.15 (Table 1), at a frequency of 6.5 Hz, the input signal into the harmonic oscillator is attenuated almost 90 percent, meaning that only about 10 percent of the input signal's amplitude remains in the output. Therefore, attempting to amplify frequencies above 6.5 Hz with the deconvolution filter may not be practical, as it is likely that above approximately 6.5 Hz, noise, rather than the signal of interest, will be amplified.

There is a second reason for having a cutoff frequency of 6.5 Hz. As will be discussed in Section 5, 31-foot vertical track wavelengths will be the smallest wavelength of interest. Maximum speeds attained during data collection were 125 miles per hour, which indicates a maximum frequency of interest of 5.9 Hz. Therefore, a cutoff frequency of 6.5 Hz, which is slightly greater than 5.9 Hz, was chosen.

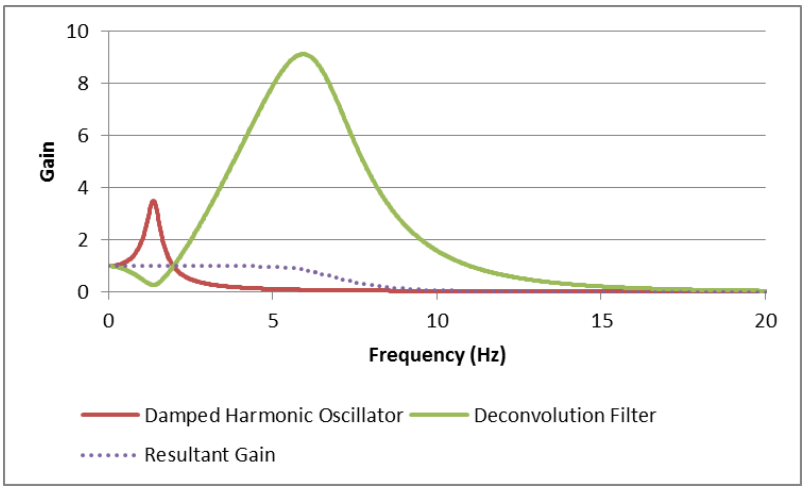

Figure 11. Frequency response of damped harmonic oscillator and deconvolution filter

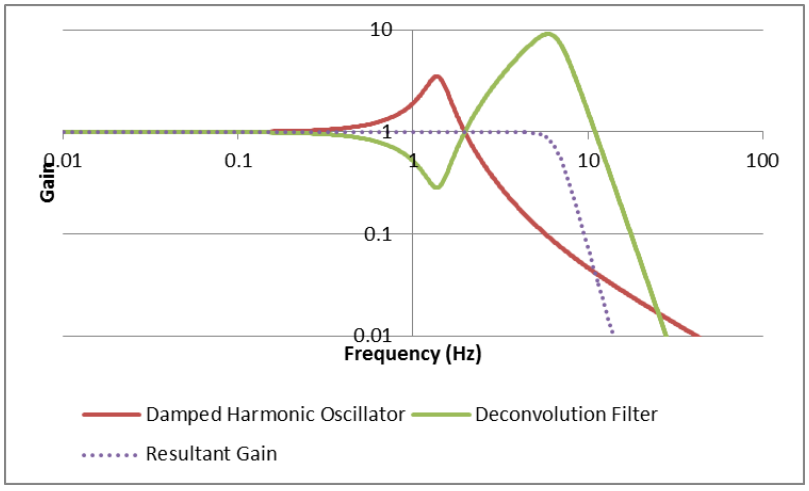

Figure 12. Frequency response of damped harmonic oscillator and deconvolution filter in log-log coordinates

In order to implement the deconvolution filter, the position, velocity, and acceleration of the harmonic oscillator sprung mass must be known. The fact that the position, velocity, and acceleration of the sprung mass must all be measured or derived is evident from the appearance of *y(t)* and the first and second derivatives of *y(t)* in Equation 7. In a real-world, data collection scenario, only the acceleration $\left(\frac{d^2y}{dt^2}\right)$ of the sprung mass (the railcar body) is typically measured. Therefore, numerical integration of the sprung mass accelerations is necessary to obtain the approximate velocity $\left(\frac{dy}{dt}\right)$ and position *y(t)* of the sprung mass. However, integration and double integration of the acceleration data can result in low frequency offsets. A band-pass Butterworth filter can be applied in order to eliminate, or at least partially eliminate, this low frequency offset. Therefore, the accelerations and derived velocity and displacement were filtered using a band-pass filter. Figure 13 shows the frequency response of the band-pass filter, and Table 4

provides the numerical values of all the poles and zeros. The gain required for this pole and zero configuration (Table 4) of the band-pass filter is $61{,}529.091 \times 10^6$.

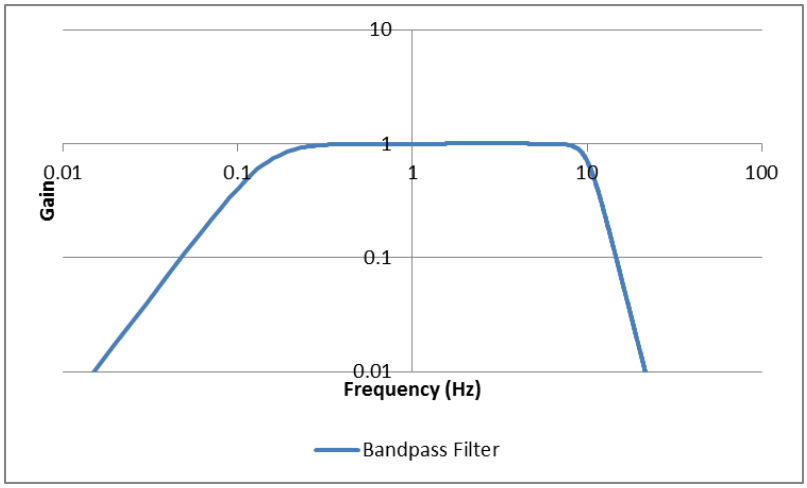

Figure 13. Frequency response of band-pass filter

Table 4. Real and imaginary components of band-pass filter poles and zeros

	Real Component	Imaginary Component
Pole #1	-0.6664	0.6664
Pole #2	-0.6664	-0.6664
Pole #3	-16.2621	60.6909
Pole #4	-16.2621	-60.6909
Pole #5	-44.4288	44.4288
Pole #6	-44.4288	-44.4288
Pole #7	-60.6909	16.2621
Pole #8	-60.6909	-16.2621
Zero #1	-4.4429E-06	4.4429E-06
Zero #2	-4.4429E-06	-4.4429E-06

The same band-pass filter (Figure 13 and Table 4) can be reapplied to the output of the deconvolution filter in order to smooth the data and eliminate long wavelengths. Figure 14 shows the suggested filter sequence.

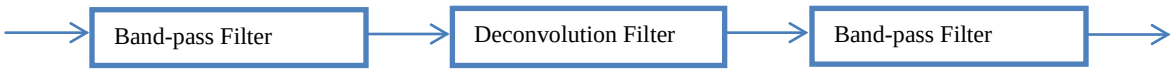

Figure 14. Sequence of filters

4. Effect of Applying the Deconvolution Filter to Measured Railcar Body Acceleration Data

This section provides several visual examples of the effects of applying the deconvolution filter to measured railcar body accelerations. Figure 15 and Figure 16 show examples of areas where the deconvolution filter (green plots) is amplifying the measured car body accelerations (red plots), and Figure 17 and Figure 18 show examples of areas where the deconvolution filter is attenuating the measured car body accelerations.

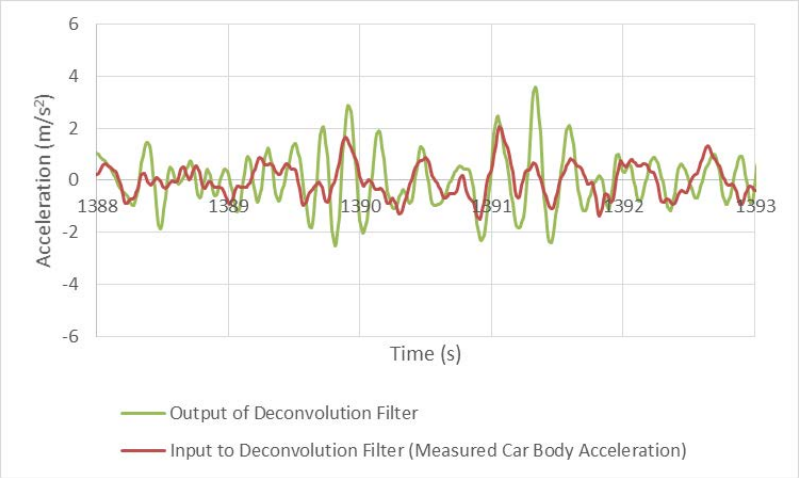

Figure 15. First example of the deconvolution filter amplifying the input signal

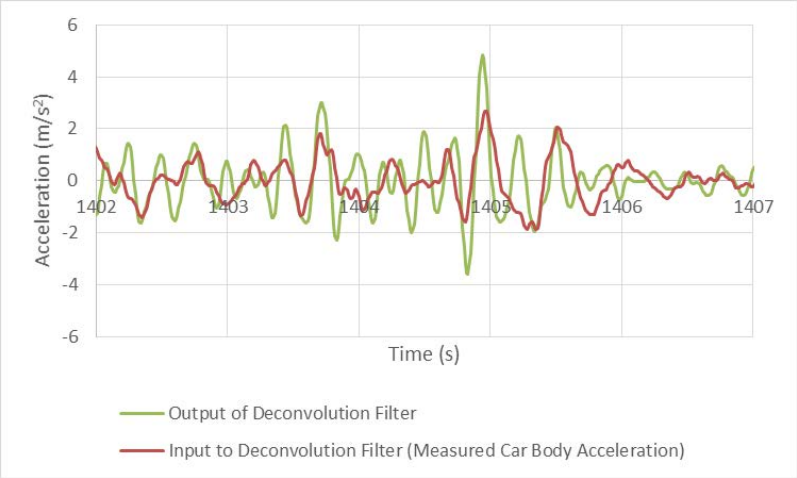

Figure 16. Second example of the deconvolution filter amplifying the input signal

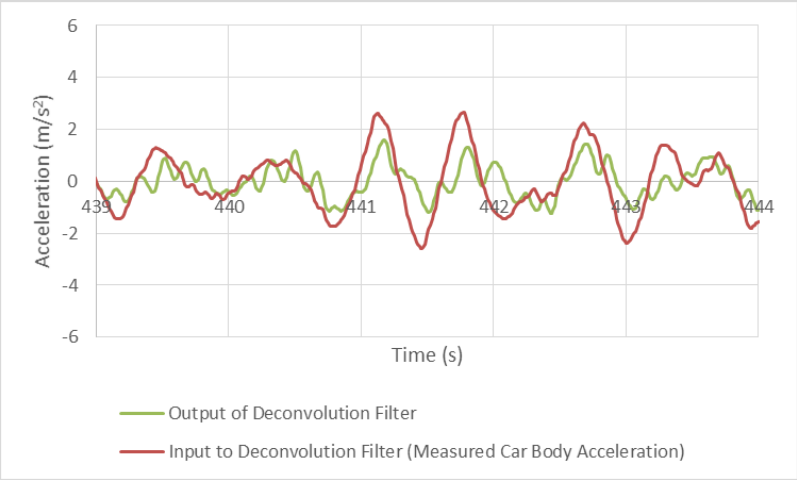

Figure 17. First example of the deconvolution filter attenuating the input signal

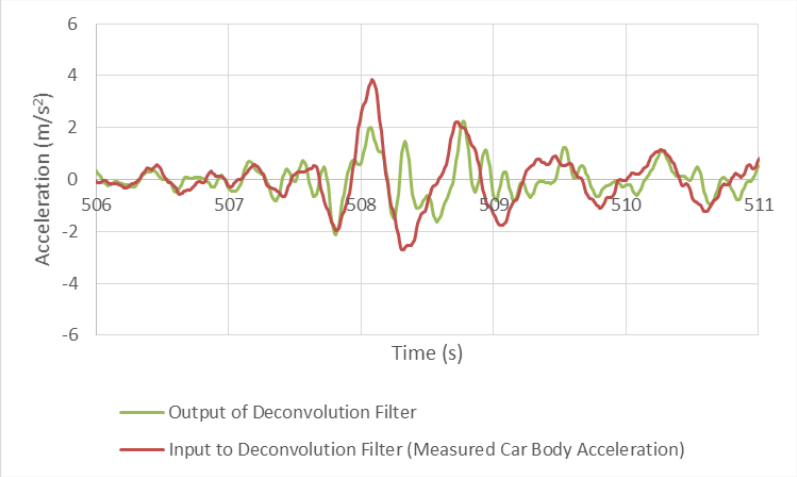

Figure 18. Second example of the deconvolution filter attenuating the input signal

These examples demonstrate that the deconvolution filter has the potential to amplify some measured railcar body accelerations and attenuate others. This is a promising sign since it is clear that the deconvolution filter is significantly modifying its input signal. With this in mind, the next step was to determine whether the deconvolution filter might be a valuable tool capable of finding vertical track geometry deviations. The next section details a data collection effort that was undertaken to gain more insight into the potential usefulness of the deconvolution filter.

5. Quantification of the Deconvolution Filter Effectiveness for Finding Track Profile Geometry Conditions

5.1 Data Collection

Amtrak inspects its Northeast Corridor high-speed passenger line between Washington, DC, and Boston, MA, every 2 weeks using a manned track geometry inspection vehicle. This vehicle is a full-size railcar typically placed at the end of an in-service passenger train consist. The track geometry system outputs multiple parameters, including but not limited to, the following:

- Left rail alinement[9] (lateral deviation of the left rail in space)
- Right rail alinement (lateral deviation of the right rail in space)
- Gage (lateral distance between the left and right rail)
- Left rail surface (vertical deviation of the left rail in space)
- Right rail surface (vertical deviation of the right rail in space)
- Cross level (vertical displacement between the left and right rail)

In addition to foot-by-foot data for the above parameters, the track geometry system also generates an exception report that includes exception magnitudes and locations for each of the parameters. In light of this, it was decided that Amtrak's geometry car would provide a good platform upon which to test the effectiveness of the deconvolution filter.

In coordination with Amtrak's engineering department, a member of FRA's research and development team was permitted to collect railcar body acceleration data on one of Amtrak's regularly scheduled geometry car runs. The data collection took place on February 5, 2014. Geometry data and acceleration data were both collected between Baltimore-Washington International (BWI) Airport and Philadelphia, and this section of track will serve as the "test zone" for analysis purposes.

Figure 19 and Figure 20 show the accelerometers used for data collection. Two accelerometers were used, but it is important to note that one accelerometer would have sufficed. Two accelerometers were used simply for purposes of redundancy. The accelerometers were placed almost directly above the front truck and as close to the centerline of the car body as possible.

[9] Historically in the railroad industry, the word has been spelled this way rather than the traditional way ("alignment").

Figure 19. Accelerometers taped down to the floor of Amtrak's geometry car

Figure 20. Close-up view of accelerometers

At the end of the data collection effort, the Amtrak engineering department provided a list of exceptions generated by the track geometry system. This list was generated using Amtrak's maintenance thresholds, which are typically 75 percent of the thresholds outlined in the Track Safety Standards.

5.2 Data Analysis Assumptions

The only geometry parameter of interest is the vertical displacement of the left and right rails. Alinement, gage, cross level, and warp will not be used in this data analysis. These parameters are not being considered because, as was pointed out previously, the deconvolution filter formulated in this paper assumes that the railcar is modeled as a single degree of freedom system in which only vertical displacements are "allowed."

Amtrak's maintenance standards are typically 75 percent of the values put forth in the Track Safety Standards. For track Classes 6 through 8, a 124-foot mid-chord offset is prescribed as well, but for the purposes of simplicity and to limit the scope of the analysis, the 124-foot chord length will not be considered. Table 5 provides Amtrak's maintenance thresholds for 31-foot and 62-foot mid-chord offsets.

Table 5. Amtrak maintenance thresholds for 31-foot and 62-foot profile deviations

Class of Track	31-Foot Mid-Chord Offset (inches)	62-Foot Mid-Chord Offset (inches)
6	0.75	0.75
7	0.75	0.75
8	0.5625	0.75

Most of the track in the test zone (BWI Airport to Philadelphia) was Class 6 or 7 track. However, there was a section of track between Baltimore and Philadelphia that was posted as Class 8. Table 5 shows that the 31-foot and 62-foot mid-chord offset thresholds are the same for Classes 6 and 7; however, for Class 8 track, the 31-foot mid-chord offset maintenance threshold is 0.5625 inches, rather than 0.75 inches. For the purposes of this analysis, it will be assumed that all track in the test zone was Class 6 or 7. This simplifies software programming for the deconvolution filter since the thresholds for Classes 6 and 7 are the same.

As was stated previously, the accelerometer used for data collection should be placed above one of the trucks and should also be placed as close to the centerline of the railcar as possible. It is important to realize that the data collected cannot distinguish the difference between a geometry deviation in the left rail and a geometry deviation in the right rail. For example, the following three scenarios would theoretically result in the same data being collected:

- 62-foot left rail deviation of 1 inch and no displacement of the right rail
- 62-foot right rail deviation of 1 inch and no displacement of the left rail
- Simultaneous 62-foot left rail and right rail deviation of 0.5 inches

The displacement parameter output by the deconvolution filter can be thought of as the average displacement of the left and right rails (Figure 21).

Figure 21. Geometry configuration of data collection with accelerometer

Therefore, when applying the deconvolution filter, it is important to realize that the thresholds in Table 5 must be halved. These thresholds for the deconvolution filter are presented in Table 6.

Table 6. Deconvolution filter thresholds for 31-foot and 62-foot profile deviations

Class of Track	31-Foot Mid-Chord Offset (inches)	62-Foot Mid-Chord Offset (inches)
6	0.375	0.375
7	0.375	0.375
8	0.28125	0.375

Because of the geometry of this data collection setup and the thresholds used for the deconvolution filter, it is clear that some false alarms can be expected. For example, using a single vertical accelerometer placed on the center line of the railcar, a dip of 1.5 inches in a single rail over 62 feet is indistinguishable from a simultaneous dip of 0.75 inches in both rails over 62 feet. The first condition (single rail dip of 1.5 inches) is in fact an FRA defect for track Classes 6 through 8, while the second condition (double rail dip of 0.75 inches) is not. However, both conditions will appear equivalent to a single vertical accelerometer placed on the center line of the railcar.

The haversine formula was used to calculate the approximate distance from the track geometry exception locations to the deconvolution filter exception locations. If the distance was less than 240 feet, a "hit" was recorded, and if the distance was greater than 240 feet, either a "miss" or "false alarm" was recorded, depending on which label was appropriate. A length of 240 feet was chosen since it represents approximately six rail lengths[10] and generally seemed to be a reasonable number. It is important to note that a distance of at least 183 feet had to be chosen since at top speeds of 125 miles per hour, the track geometry car was traveling at 183 feet per second.[11] GPS only samples at 1 Hz. Therefore, at top speeds there were up to 183 feet between GPS locations. Furthermore, only sections of the test zone where speeds exceeded 60 miles per hour were considered.

5.3 Results

5.3.1 Signal Detection Theory

Signal detection theory can be used to quantify the sensitivity of the deconvolution filter to vertical track geometry conditions.[12] The track profile exceptions from the track geometry

[10] Traditionally, track with jointed rail (as opposed to continuously welded rail) is composed of 39-foot long rail segments.

[11] The data collection was conducted on Amtrak's regional geometry car, but if the data had been collected on Amtrak's Acela geometry car, top speeds of 150 miles per hour (220 feet per second) would have been experienced.

[12] There are several references, such as Macmillan & Creelman (2005), that provide a good introduction to signal detection theory. In addition, Appendix A includes a brief one page summary of some important equations in signal detection theory.

exception list will serve as the "ground truth". Table 7 shows the *d'* sensitivity values, as well as the true positive rate and false positive rate, for the 31-foot track profile deviations when using the Amtrak maintenance threshold (shaded row) and five additional thresholds. The *d'* values for these five additional thresholds were determined in order to obtain more data points with which to form a receiver operating characteristic (ROC) curve for 31-foot vertical track deviations and 62-foot vertical track deviations. Table 8 shows the equivalent information for 62-foot track profile deviations. Appendix B provides the number of hits, misses, false alarms, and correct rejections for each of the cases presented in Table 7 and Table 8.

Table 7. Signal detection theory results for 31-foot MCO sensitivity

Threshold as Percentage of Amtrak Maintenance Threshold	Sensitivity (*d'*)	False Positive Rate	True Positive Rate
50%	2.53	0.169	0.942
67%	2.39	0.082	0.842
80%	2.14	0.037	0.640
100%	1.95	0.010	0.360
120%	2.32	2.92x10-4	0.132
133%	1.89	2.92x10-4	0.061

Table 8. Signal detection theory results for 62-foot MCO sensitivity

Threshold as Percentage of Amtrak Maintenance Threshold	Sensitivity (*d'*)	False Positive Rate	True Positive Rate
50%	2.10	0.311	0.946
67%	2.70	0.155	0.954
80%	2.62	0.090	0.900
100%	2.66	0.037	0.808
120%	2.44	0.010	0.554
133%	2.42	0.003	0.392

Figure 22 shows the sensitivity values from Table 7 and Table 8 on an ROC plot. The blue and red curves represent curves of constant sensitivity (commonly known as isosensitivity curves) for 31-foot profile and 62-foot profile detection, respectively. The dotted line (Figure 22) represents an isosensitivity curve for a system that is completely insensitive to a given condition. Therefore, in layman's terms, the farther away an isosensitivity curve is from the zero sensitivity curve (dotted line in Figure 22), the better the sensitivity of the system. The six blue diamonds and the six red squares represent the false positive rates and true positive rates put forth in Table 7 and Table 8. Figure 22 and the numbers in Table 7 and Table 8 show that as the threshold is

lowered, the false alarm rate rises, as does the hit rate. Therefore, as the threshold is lowered, the bias[13] to say "Yes, the threshold has been exceeded," is increased.

Figure 23 provides equivalent information to Figure 22 but uses z-coordinates which can sometimes make it easier to see the difference in sensitivity since the isosensitivity curves (Figure 22) become straight lines.

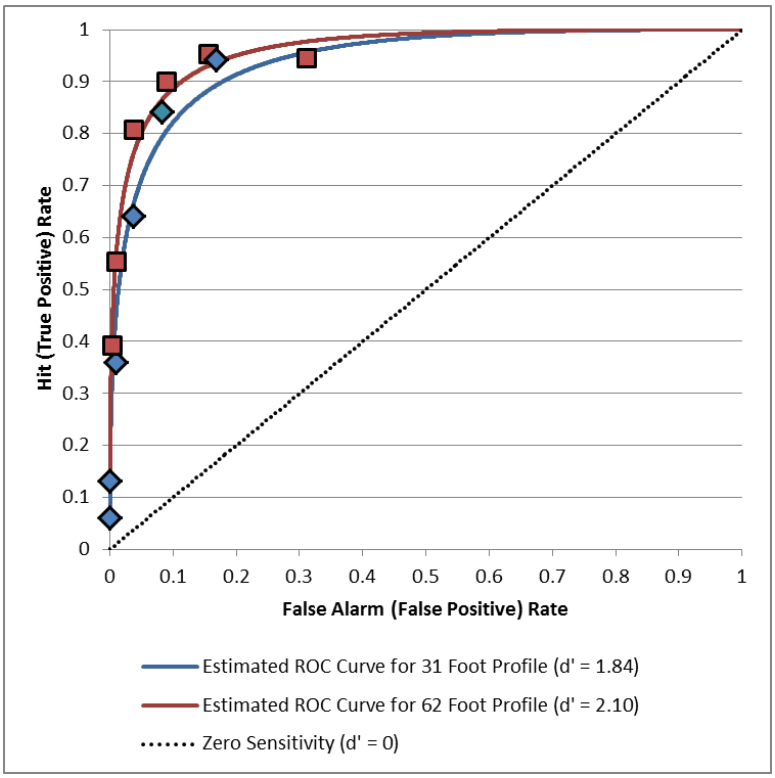

Figure 22. Receiver operating characteristic (ROC) curves

[13] "Bias" is a signal detection theory term that is explained in more detail in textbooks on signal detection theory, such as Macmillan & Creelman (2005).

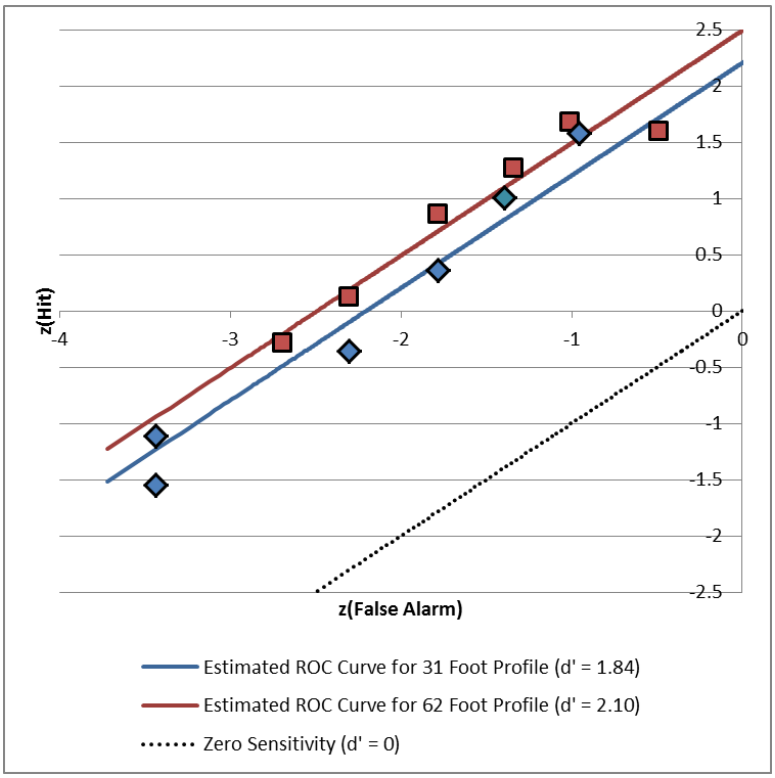

Figure 23. Receiver operating characteristic (ROC) curves in z-coordinates

The deconvolution filter appears to be slightly more effective at finding 62-foot profile exceptions than 31-foot profile exceptions. A t-test was performed to compare the six 31-foot profile *d'* values (Table 7) with the six 62-foot profile *d'* values (Table 8). A p-value below 0.05 was calculated, which indicates that there is a statistically significant difference in the two sets of *d'* values.

There may be a logical explanation for the higher sensitivity of the deconvolution filter to 62-foot wavelengths. The deconvolution filter was formulated assuming the railcar is a harmonic oscillator (Figure 1). One of the assumptions behind this harmonic oscillator configuration is a single (or point) contact between the mass and the base, or in the case of a railcar, between the car body and the track (Figure 24). However, the configuration shown in Figure 24 is clearly not accurate since typical railcars have two trucks, and each truck has two axles (Figure 25). The truck center to truck center spacing is typically 59.5 feet.

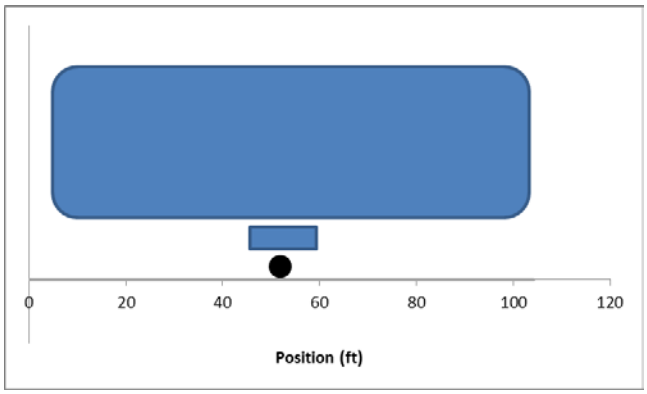

Figure 24. Assumed railcar configuration

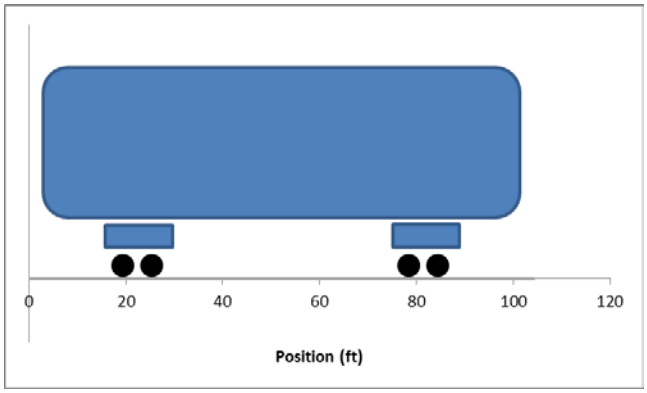

Figure 25. Typical railcar configuration

Figure 26 and Figure 27 show a railcar over a 31-foot and a 62-foot wavelength, respectively. When the wavelength in the track becomes shorter than the distance between the two trucks (typically 59.5 feet), then the assumption of a single point contact is less valid. For example, in the case of a 31-foot wavelength (Figure 26), it is clear that each truck will individually experience the 31-foot deviation. However, in the case of a 62-foot deviation, the assumption of a single point contact is more appropriate since both trucks experience the 62-foot wavelength nearly simultaneously (Figure 27). Therefore, it makes sense that the deconvolution filter would be more sensitive to 62-foot wavelengths than to 31-foot wavelengths because a railcar traversing a 62-foot wavelength is more in line with the single point of contact harmonic oscillator on which the deconvolution filter design is based.

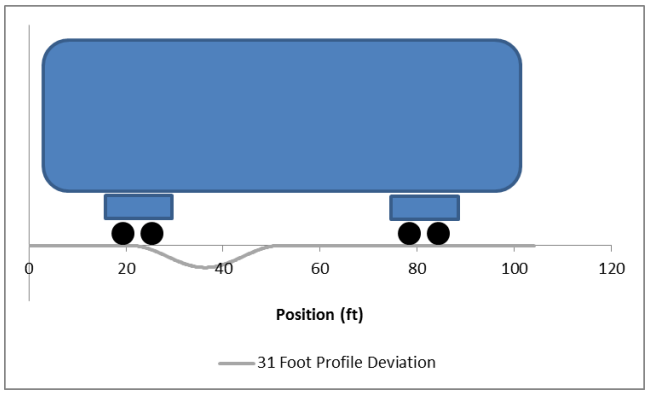

Figure 26. Railcar over a 31-foot track wavelength

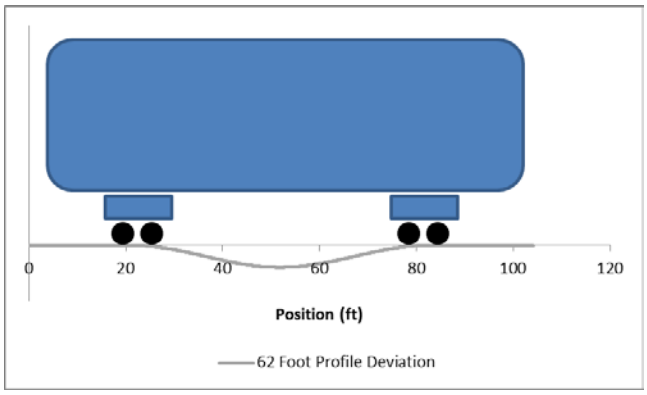

Figure 27. Railcar over a 62-foot track wavelength

5.3.2 Comparison to Traditional Methods

Traditionally, when measuring railcar body accelerations, a 10 Hz low-pass filter is applied to the measured car body accelerations. Then a peak-to-peak threshold of 0.6 g (or sometimes a higher value, such as 0.9 g), along with a 1-second moving window, is used as a metric to determine the locations for ground verification on the track. It is interesting to note that using this approach would have resulted in no exception locations in the test zone. In other words, there would have been zero hits and zero false alarms, but there would have been 133 misses in the case of the Amtrak maintenance threshold for 62-foot chords and 119 misses in the case of the Amtrak maintenance threshold for 31-foot chords. In other words, this traditional approach of simply using a low-pass filter along with a peak-to-peak threshold value is not fully effective at locating track geometry conditions.

5.3.3 Example Waveform from Exception Location Chosen at Random

One exception location was chosen at random in order to visualize the acceleration and displacement waveforms. The location chosen was flagged by the geometry system as a 62-foot right rail surface deviation of 0.98 inches, which exceeds Amtrak's maintenance threshold of 0.75 inches (Table 5). The location was also flagged by the deconvolution filter as a maintenance location with 0.38 inches displacement; the threshold for the deconvolution filter was 0.375 inches (Table 6) which is half the Amtrak maintenance threshold of 0.75 inches. The location of the exception was approximately 1,540 feet from milepost 85. The latitude and longitude coordinates are 39.335007 and -76.431158, respectively. Figure 28 shows an overview image of the exception location.

Figure 28. Overhead view of example exception location

Figure 29 shows a zoomed-out view of the railcar body acceleration waveform and the acceleration and displacement waveforms output by the deconvolution filter from the exception location. Three thousand feet (0.57 miles) of data is shown in Figure 29. Figure 30 is a zoomed-in view of the same exception location, with 100 feet of data shown. If one were looking only at railcar body accelerations (red plot in Figure 29 and Figure 30) to try and determine poor track conditions, this location would likely not be flagged. There is a "blip" in the railcar body accelerations, but it only has a peak-to-peak magnitude of slightly more than 1.5 meter per second squared, which is approximately equal to 0.15 g. However, the accelerations output by the deconvolution filter (green plot in Figure 29 and Figure 30) clearly amplify this location.

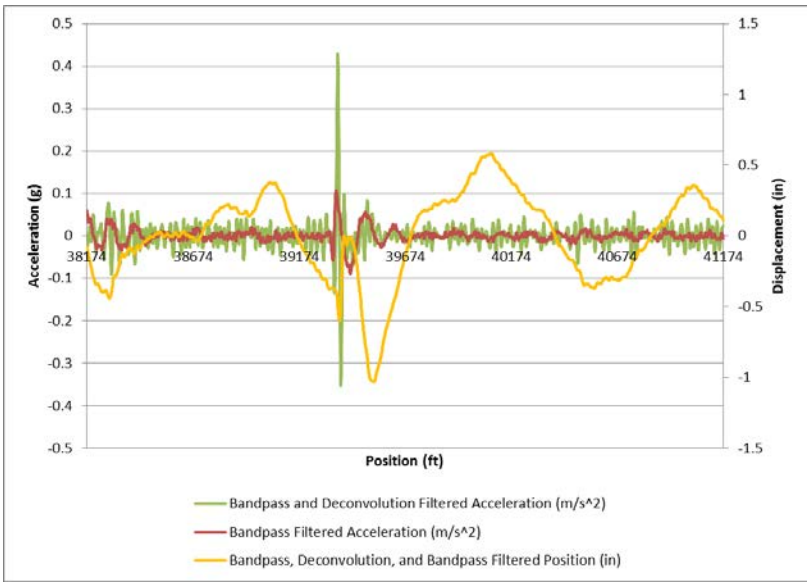

Figure 29. Zoomed-out view of exception location

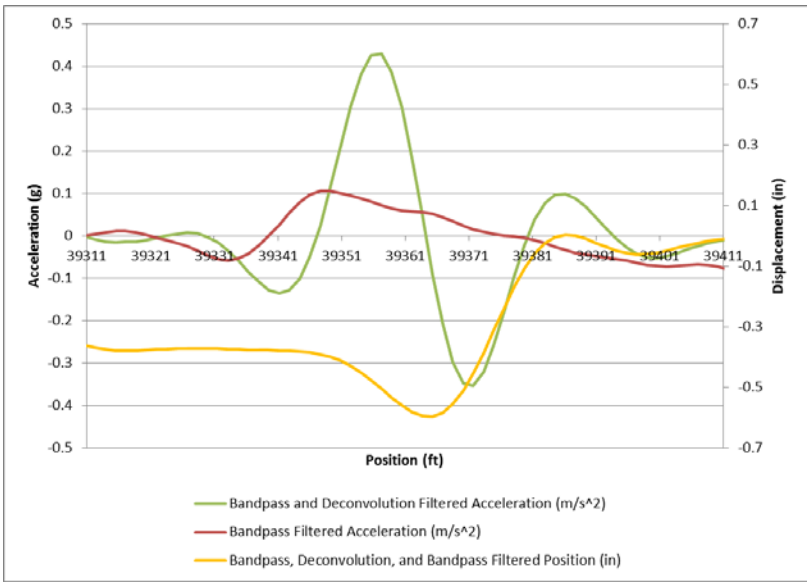

Figure 30. Zoomed-in view of exception location

There is also a sudden change in displacement output by the deconvolution filter (orange line in Figure 29 and Figure 30). This sudden change in displacement results in a 62-foot mid-chord offset (MCO) of 0.38 inches (dotted blue line in Figure 31), which is slightly greater than the threshold value of 0.375 (which is half of Amtrak's 0.75-inch maintenance threshold).

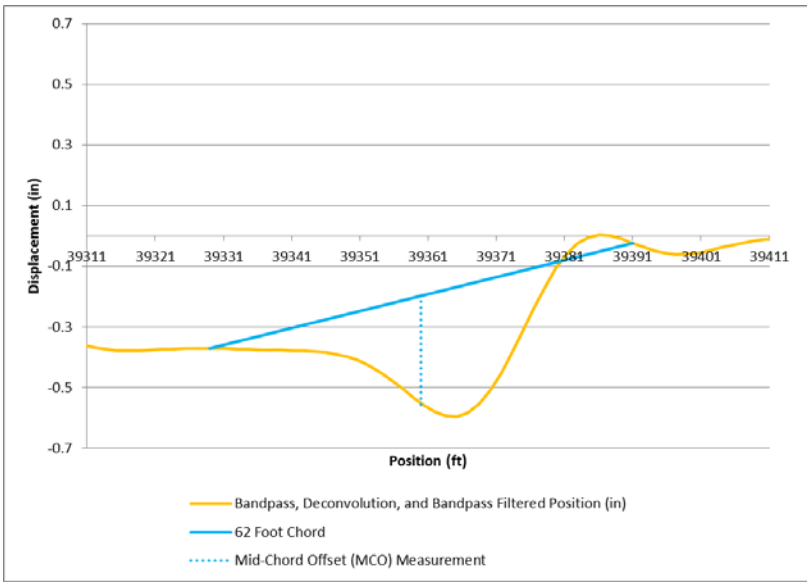

Figure 31. Displacement waveform at exception location with mid-chord offset

6. Conclusions

The data collection and analysis presented in this paper demonstrate that the deconvolution filter appears to be a better method of detecting track geometry profile exception locations when compared with the simpler, traditional method of using peak-to-peak measured railcar body acceleration data magnitudes as an indication of poor track conditions. In the future, additional data collection on other types of rail vehicles, such as locomotives, will likely be pursued in order to further validate the positive results that have been discussed in this report. In addition, data collection on more than one vehicle in a single train consist might be considered in order to determine the repeatability of the data output by the deconvolution filter, as well as determine the effect of individual railcar characteristics on the output of the filter. Also, FRA will consider investigating the effectiveness of the deconvolution filter at detecting 124-foot wavelength track deviations.[14]

If promising results from the deconvolution filter are obtained, real-time implementation of the filter will be considered. A potential system for real-time implementation was developed previously by FRA Research and Development (FRA Research Results RR 12-19). This system was used in the data collection effort on the Amtrak geometry car documented earlier in this report. Several issues would have to be addressed if implementation of the filter in real-time were to be pursued. One of the main issues will be whether to assume a natural frequency based on the type of vehicle on which data is being collected, or whether to numerically calculate the natural frequency (using an FFT algorithm, for example) in real-time in order to estimate the natural frequency of the specific railcar on which data is being collected. The latter approach was used in the analysis presented in this report (Figure 2), but the calculation of the FFT was done manually rather than in an integrated fashion with the deconvolution filter.

[14] A 124-foot mid-chord offset measurement is called for in the high speed Track Safety Standards (49 CFR 213, Subpart G).

Appendix A. Brief Background on Signal Detection Theory

In signal detection theory, the outcome of a "yes-no" experiment falls into one of four categories:

- Hit (or true positive)
- False alarm (or false positive)
- Miss (or false negative)
- Correct rejection (or true negative)

Table A.1 summarizes these four categories.

Table A.1. Signal detection theory categories

		Response of Observer	
		"Yes"	"No"
State of World	Defect	Hit (True Positive)	Miss (False Negative)
	No Defect	False Alarm (False Positive)	Correct Rejection (True Negative)

The following formulas relate the probability of a hit to the probability of a miss and the probability of a false alarm to the probability of a correct rejection:

$$p(\text{Hit}) + p(\text{Miss}) = 1$$
$$p(\text{False Alarm}) + p(\text{Correct Rejection}) = 1$$

In signal detection theory, the sensitivity (commonly denoted by the symbol *d'* and pronounced "dee-prime") is defined using the following formula:

$$d' = z[p(\text{Hit})] - z[p(\text{False Alarm})]$$

where z[p(Hit)] is the inverse of the normal distribution function (z score) associated with p(Hit), and z[p(False Alarm)] is the z score associated with p(False Alarm). Given a specified probability, the z score is the corresponding x-axis value of the standard normal distribution.

Another parameter, commonly known as the percent correct or accuracy, can be used to determine the effectiveness of a system at detecting a certain condition. The accuracy parameter is a less rigorous but more intuitive measure of sensitivity than *d'*. The percent correct or accuracy is calculated using the following formula:

$$\text{Accuracy} = \frac{(\text{Hits}) + (\text{Correct Rejections})}{(\text{Hits}) + (\text{Correct Rejections}) + (\text{Misses}) + (\text{False Alarms})}$$

Appendix B. Number of Hits, Misses, False Alarms, and Correct Rejections

Table B.1 shows the number of hits, misses, false alarms, and correct rejections for the deconvolution filter when using Amtrak maintenance thresholds for 31-foot deviations, and Table B.2 shows the same information for 62-foot deviations. These numbers (along with the signal detection theory formulas put forth in Appendix A) were used to determine the *d'* values put forth in Table 7 and Table 8. The number of correct rejections was calculated by breaking the test zone (where speeds exceeded 60 miles per hour) up into 240-foot segments, which resulted in 1,848 segments. Then the number sum of the hits, misses, and false alarms was subtracted from 1,848 in order to determine the number of correct rejections. This is not a rigorous approach but will suffice for the purposes of this report.

Table B.1. Number of hits, misses, false alarms, and correct rejections for 31-foot deviations

Threshold as Percent of Amtrak Maintenance Threshold	Number of Hits	Number of Misses	Number of False Alarms	Number of Correct Rejections
50%	131	8	289	1420
67%	117	22	140	1569
80%	89	50	64	1645
100%	50	89	18	1691
120%	18.5	121.5	0.5[15]	1709.5
133%	8.5	131.5	0.5	1709.5

[15] The 120 percent and 133 percent thresholds for 31-foot deviations had zero false alarms which led to a false alarm rate equal to zero for both of these thresholds. The equation for calculating the *d'* sensitivity parameter requires a non-zero false alarm rate as well as a non-zero hit rate. Therefore, a value of 0.5 was added to the hits, misses, false alarms, and correct rejections in the 120 percent threshold row and the 133 percent threshold row in Table B.1.

Table B.2. Number of hits, misses, false alarms, and correct rejections for 62-foot deviations

Threshold as Percent of Amtrak Maintenance Threshold	Number of Hits	Number of Misses	Number of False Alarms	Number of Correct Rejections
50%	123	7	535	1183
67%	124	6	266	1452
80%	117	13	154	1564
100%	105	25	63	1655
120%	72	58	18	1700
133%	51	79	6	1712

References

Al-Nazer, Leith & Borgovini, Robert J. *Development of an Ultra-Portable Ride Quality Meter*. FRA Research Results RR 12-19, December 2012.

Hartog, J.P. Den. *Mechanical Vibrations*. Dover Publications, 1985.

Lathi, B.P. *Linear Systems and Signals (Second Edition)*. Oxford University Press, 2004.

LePage, Wilbur R. *Complex Variables and the Laplace Transform for Engineers*. Dover Publications, 1980.

Macmillan, Neal A. & Creelman, Douglas C. D*etection Theory: A User's Guide (Second Edition)*. Mahwah, New Jersey: Lawrence Erlbaum Associates Publishers, 2005.

Rao, Singiresu S. *Mechanical Vibrations*. Reading, Massachusetts: Addison-Wesley Publishing Company, 1986.

Abbreviations and Acronyms

CFR	Code of Federal Regulations
FFT	Fast Fourier Transform
FRA	Federal Railroad Administration
MCO	Mid-Chord Offset
ROC	Receiver Operating Characteristic
TSS	Track Safety Standards